International Journal of
*Molecular Sciences*

MDPI

*Article*

# Investigating Amphoteric 3,4′-Biscoumarin-Based *ortho*-[(Dialkylamino)methyl]phenols as Dual MAO and ChE Inhibitors

**Anthi Petrou [1,†], Caterina Deruvo [2,†], Rosa Purgatorio [2], Boris Lichitsky [3], Andrey N. Komogortsev [3], Victor G. Kartsev [4], Modesto de Candia [2], Marco Catto [2], Cosimo D. Altomare [2,*] and Athina Geronikaki [1,*]**

1 Department of Pharmaceutical Chemistry, School of Pharmacy, Aristotle University of Thessaloniki, 54124 Thessaloniki, Greece; anthi.petrou.thessalonik1@gmail.com
2 Department of Pharmacy-Pharmaceutical Sciences, University of Bari Aldo Moro, Via E. Orabona 4, 70125 Bari, Italy; caterina.deruvo@uniba.it (C.D.); rosa.purgatorio@uniba.it (R.P.); modesto.decandia@uniba.it (M.d.C.); marco.catto@uniba.it (M.C.)
3 Zelinsky Institute of Organic Chemistry, Leninsky Prospect, 119991 Moscow, Russia; blich2006@mail.ru (B.L.); dna5@mail.ru (A.N.K.)
4 InterBioScreen Ltd., 119019 Moscow, Russia; vkartsev@ibscreen.chg.ru
* Correspondence: cosimodamiano.altomare@uniba.it (C.D.A.); geronik@pharm.auth.gr (A.G.); Tel.: +39-080-544-2781 (C.D.A.); +30-231-099-7616 (A.G.)
† These authors contributed equally to this work.

## Abstract

Nineteen previously and newly synthesized amphoteric 8-[(dialkylamino)methyl]-7-hydroxy-4-(2-oxo-2*H*-chromen-3-yl)-2*H*-chromen-2-ones were assayed as inhibitors of monoamine oxidases (MAO-A and B) and cholinesterases (AChE and BChE). Five of the tested compounds (**2b**, **2c**, **3c**, **5b**, and **5c**), namely those bearing the less bulky alkyls in the Mannich base 8-$CH_2NR_2$ (R = Me, Et) and the halogens (Cl, Br) at C6 of the 4-coumarin-3-yl moiety, showed moderate inhibitory potencies toward human MAO-A in the single-digit micromolar range ($IC_{50}$s from 1.49 to 3.04 μM). In particular, the 6′-Cl derivatives **2b** and **5b** proved to be reversible competitive inhibitors of human MAO-A with $K_i$ values of 0.272 and 0.326 μM. Among the tested compounds, **3c** proved to also be a moderate inhibitor of human AChE ($IC_{50}$ 4.27 μM). Molecular docking calculations suggested binding modes of the most active compounds to MAO-A and AChE binding sites consistent enough with the experimental data. Chemoinformatic tools suggest for the most active compounds, including the dual MAO-A/AChE inhibitor **3c**, full compliance with Lipinski's rule of five, high probability of gastrointestinal absorption, but low blood–brain barrier (BBB) permeability. While further efforts are required to improve their CNS distribution, herein new phenolic Mannich bases have been identified that may have potential for treating neurodegenerative syndromes.

**Keywords:** biscoumarin; monoamine oxidases; cholinesterases; inhibitors; molecular docking; ADME profile; Alzheimer's disease

check for updates

Academic Editor: Cheng-Yang Huang

Received: 1 August 2025
Revised: 10 October 2025
Accepted: 13 October 2025
Published: 20 October 2025

**Citation:** Petrou, A.; Deruvo, C.; Purgatorio, R.; Lichitsky, B.; Komogortsev, A.N.; Kartsev, V.G.; de Candia, M.; Catto, M.; Altomare, C.D.; Geronikaki, A. Investigating Amphoteric 3,4′-Biscoumarin-Based *ortho*-[(Dialkylamino)methyl]phenols as Dual MAO and ChE Inhibitors. *Int. J. Mol. Sci.* **2025**, *26*, 10197. https://doi.org/10.3390/ijms262010197

**Copyright:** © 2025 by the authors. Licensee MDPI, Basel, Switzerland. This article is an open access article distributed under the terms and conditions of the Creative Commons Attribution (CC BY) license (https://creativecommons.org/licenses/by/4.0/).

## 1. Introduction

Alzheimer's disease (AD) is the leading neurodegenerative disease, with a strong impact on health and quality of life. People suffering from AD have learning deficits along with an impairment of memory and language skills due to the disruption of cholinergic transmission in hippocampal areas [1]. As a result of the so-called 'cholinergic hypothesis',

up to date, the pharmacological therapy of AD has essentially been based on the restoration of adequate levels of acetylcholine (ACh) ensured by acetylcholinesterase (AChE) inhibitors (i.e., rivastigmine, galantamine, and donepezil) [2], but also butyrylcholinesterase (BChE) inhibitors. Memantine, an antagonist of the NMDA (*N*-methyl-D-aspartate) receptor, is also used in the therapy of moderate to severe forms of AD [3]. Nevertheless, all the mentioned drugs do not cure the disease but exert only symptomatic relief. Therefore, the need for new drugs against AD remains a challenging task. Monoclonal antibodies, such as aducanumab, lecanemab, and donanemab [4], deserve great hope as disease-resolving therapies, but approved therapies have so far shown contrasting results in terms of efficacy and harmful side effects.

In the last two decades, the multitarget approach to drug design has been considered as a promising strategy in discovering neurotherapeutics against AD [5], paying attention to other related mechanisms of neurotoxicity. In particular, oxidative stress has been considered an interplaying event with the deposition of amyloid plaques and neurofibrillary tangles [6]. In turn, deregulation of endogenous redox systems and overproduction of radical species lead to lipid peroxidation and nucleic acid mutations. In this context, a neuroprotective activity against oxidative stress has been claimed for inhibitors of monoamine oxidases. The flavoenzyme monoamine oxidase (MAO, EC 1.4.3.4), which catalyzes the oxidative deamination of dietary and neurotransmitter amines, including serotonin, tryptamine, dopamine, norepinephrine, epinephrine, β-phenylethylamine, tyramine, and octopamine, has been considered as an anti-AD drug target. MAO exists in two isoforms, MAO-A and MAO-B, sharing about 70% sequence identity and showing distinct substrate and inhibitor specificities [7]. MAO-A preferentially metabolizes serotonin and norepinephrine, while MAO-B preferentially metabolizes phenylethylamine, benzylamine, and dopamine.

According to their selectivity, MAO subtypes are involved in various neurodegenerative pathologies, including AD, Parkinson's disease (PD), and depression. Age-related increase in MAO expression levels is a significant causative factor in the etiology of neurodegenerative illnesses and mental disorders. Selective MAO-A inhibitors (MAOAIs) find use in the treatment of depression, whereas MAOBIs are used in alternation to levodopa to treat PD. First-generation MAO inhibitors, such as iproniazid, phenelzine, and tranylcypromine, are not isoform-selective and their use was associated with severe side effects [8]. Currently, selective MAOAIs (moclobemide) and MAOBIs (L-deprenyl and safinamide) are preferred because of their better therapeutic index, but with limited prevalence compared with safer and more effective drugs. Recently, a possible repositioning of MAOs as a target in chemoresistant tumors has boosted a renewed attention in MAO inhibitors, particularly for MAOAIs that have demonstrated synergistic efficacy in the antitumor therapy of recurrent prostate cancer, metastatic breast cancer, and glioma [9].

Among the numerous MAOIs developed, coumarin-based derivatives are well-documented MAO inhibitors with good MAO-A/B selectivity ratios, depending upon the nature and pattern of their substitution, and great potential as multitarget agents for neurodegenerative diseases [10]. Coumarins have a high electron count and exhibit good charge transport capabilities [11]. The coumarin moiety taken as a scaffold is synthetically versatile and widely used in the preparation of biologically active molecules. Indeed, coumarin derivatives have found a wide variety of applications for their anticoagulant, anti-inflammatory, anticancer, antidiabetic, anti-neurodegenerative, antioxidant, antidepressive, and antimicrobial effects [12]. Coumarin dimers (i.e., biscoumarins), mostly of natural origin, also form a bioactive scaffold. Very often these are symmetrical homodimers, like, for example, dicoumarol and its substituted derivatives [13,14], 3,3′-biisofraxidin (from *Sarcandrae Herba*) [15] and 4,4′-biisofraxidin (from *Impatiens balsamina*) [16], 8,8′-

biscoumarins like toddalosin (from *Toddalia asiatica*) [17], and the mycotoxins kotanin and desmethylkotanin (from *Aspergillus glaucus*) [18] (Figure 1). Biscoumarins also attracted significant interest due to their wide range of biological activities such as antimicrobial [19], anti-inflammatory [20], anticancer [21], anti-obesity [22], antiviral [23,24], antidiabetic [25], MAO inhibitory [26], and anticholinesterase [27–29] activities.

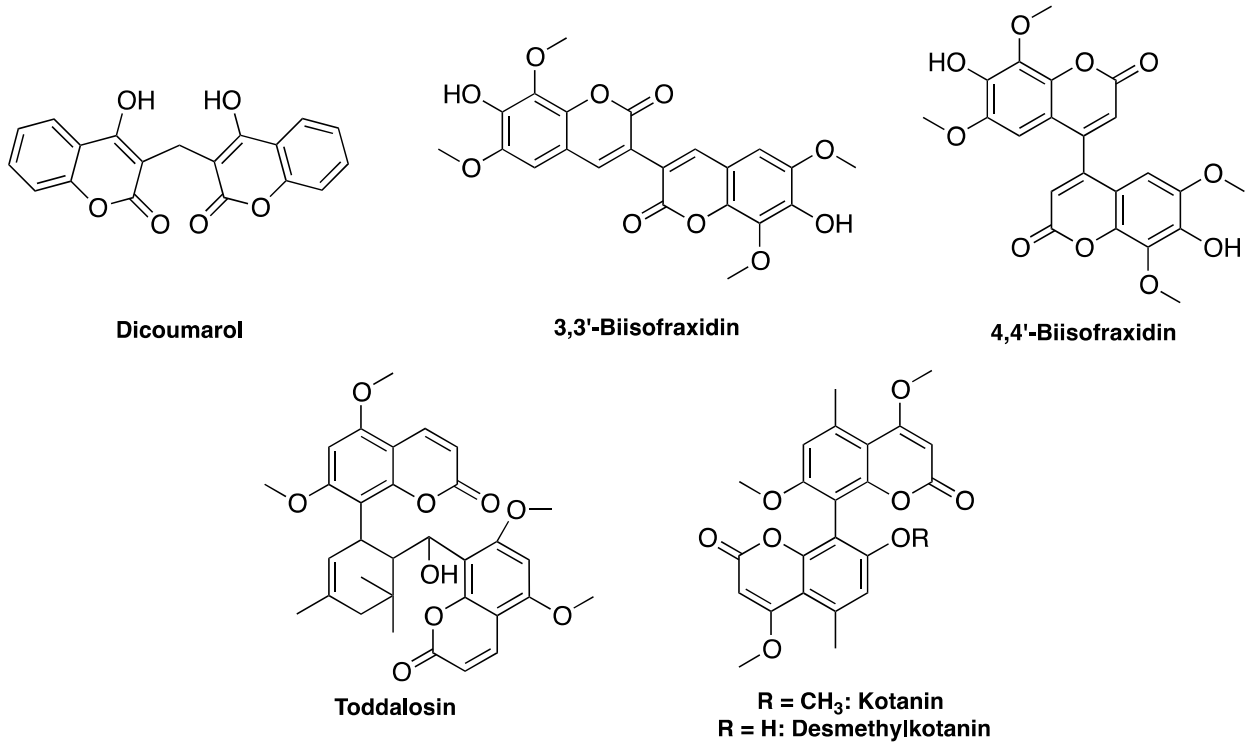
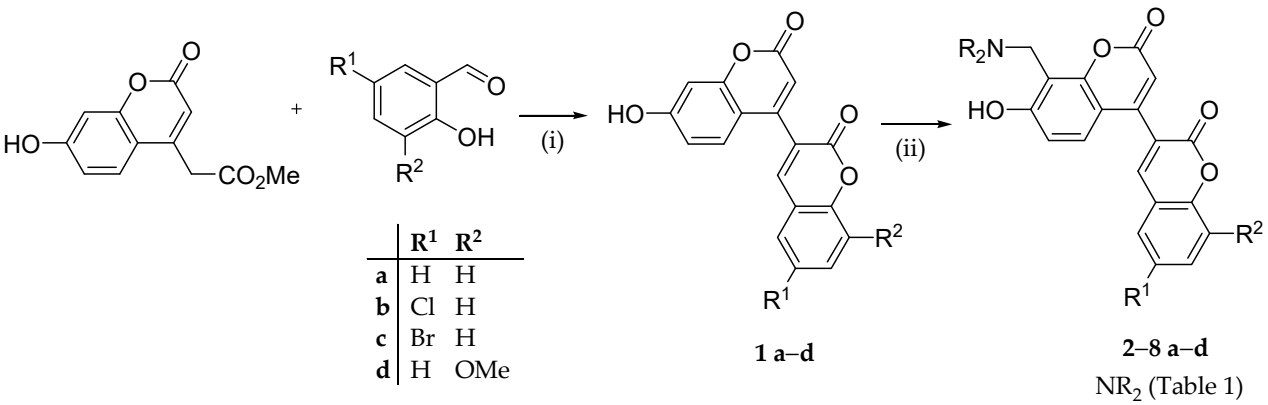



**Figure 1.** Representative structures of biologically active biscoumarin derivatives.

Several years ago, Frasinyuk et al. reported the aminomethylation of 7-hydroxy-4-(2-oxo-2*H*-chromen-3-yl)-2*H*-chromen-2-one (Scheme 1) [30], synthesizing diverse amphoteric *ortho*-phenolic Mannich bases (i.e., 8-[(dialkylamino)methyl]-7-hydroxy substituents) on the 2*H*,2′*H*-3,4′-bichromene-2,2′-dione (hereinafter referred to as 3,4′-biscoumarin) scaffold. The online PASS (prediction of activity spectra for substances) software (https://way2drug.com/PassOnline/, accessed on 20 June 2025) [31] predicted for forty diverse amphoteric 3,4′-biscoumarin derivatives indicated above MAO inhibitory activity with a Pa value (i.e., the probability of a compound to be active) in the range 0.203–0.895. Note that most of the compounds had Pa values lower than 0.5, indicating on one hand their relative novelty compared to the molecular structures in the PASS training set and on the other hand, the low probability of being active as MAOIs.

Due to our interest toward novel coumarin cores as a scaffold of novel MAOIs, endowed with further anti-AD activities, such as ChE inhibition, herein we screened nineteen previously and newly synthesized 3,4′-biscoumarins bearing the amphoteric 8-[(dialkylamino)methyl]-7-hydroxy group as dual MAO/ChE inhibitors, along with docking calculation, solubility determination, and in silico drug-likeness.




| | $R^1$ | $R^2$ |
|---|---|---|
| **a** | H | H |
| **b** | Cl | H |
| **c** | Br | H |
| **d** | H | OMe |

**Scheme 1.** Synthesis scheme of 8-[(dialkylamino)methyl]-4-(2-oxo-2*H*-chromen-3-yl)-7-hydroxy-2*H*-chromen-2-one derivatives. Reagents and conditions: (i) DBU, abs. 1,4-dioxane (DMF for **1d**), 100–105 °C, 4–10 h; (ii) suitable aminal, 1,4-dioxane, reflux, 3–5 h.

## 2. Results and Discussion

### *2.1. Chemistry*

Nine new 3,4′-biscoumarin-containing amphoteric derivatives (**2a–d**, **3c**, **4d**, **5d**, **6d**, and **8d**) were synthesized as previously described [30] according to Scheme 1. 7-hydroxy-3,4′-biscoumarins (**1a–d**) were prepared by the condensation of 7-hydroxy-coumarin-4-methylacetate with substituted salicylic aldehydes in dioxane (or DMF for **1d**) in the presence of DBU (1,8-diazabicyclo [5.4.0]undec-7-ene) as a catalyst. Regarding the aminomethylation procedure, the aminals of the secondary amines were refluxed in dioxane with a product yield between 48 and 82%. In this case, the electrophilic substitution took place exclusively at C8, as confirmed by the NMR spectra [30].

The structural exploration was primarily focused on the variation in terms of the hydrophobicity and steric effects of the alkyls of the aminomethyl group at C8 ($CH_2NR_2$) of the coumarin moiety. The congeners (**b–d**), bearing the halogens Cl or Br (as $R^1$) at C6 and OMe (as $R^2$) at C8 of the coumarin-3-yl moiety, available in our molecular library, were also investigated.

### *2.2. Structure–Activity Relationships*

#### 2.2.1. In Vitro Inhibition of Monoamine Oxidases and Cholinesterases

All nineteen compounds were tested against each enzyme, i.e., human *hu*MAO-A and *hu*MAO-B isoforms, electric eel *ee*AChE, and horse serum *eq*BChE, at 10 μM concentration, and for those exhibiting more than 60% inhibition at that concentration, the $IC_{50}$ values were determined. The inhibition of human *hu*AChE was also evaluated for five compounds. Clorgiline and donepezil were used as positive controls in the MAO and ChE inhibition assays, respectively. The enzymes' inhibition data (expressed as $IC_{50}$s or % inhibition at 10 μM concentration) are summarized in Table 1 as mean ± SD from three independent experiments.

For the sake of clarity, the position of the Mannich base (-$CH_2NR_2$) on the main coumarin core will be indicated as C8, whereas the positions of Cl or Br and OMe on the 4-coumarin-3-yl moiety will be indicated as C6′ and C8′. As can be seen in Table 1, about half of the screened compounds significantly inhibited the two MAO isoforms at 10 μM concentration, achieving a slight selectivity toward MAO-A. The most potent MAO-A inhibitors were **2b** ($IC_{50}$ 1.49 μM) and **5b** ($IC_{50}$ 1.85 μM) bearing $NMe_2$ and N(Me)*n*Bu, respectively, as $NR_2$ at C8 and Cl as $R^1$ at C6′. The inhibition kinetics determined on MAO-A for the most potent inhibitors **2b** and **5b** assessed a competitive mode of inhibition, with no variation in $v_{max}$ upon increasing the inhibitors' concentration (Figure 2). The

inhibition constant ($K_i$) values for **2b** and **5b** resulted in 0.272 ± 0.043 and 0.326 ± 0.035 μM, respectively.

**Table 1.** Monoamine oxidases (MAO A and B) and cholinesterases (AChE and BChE) inhibition data of 8-[(dialkylamino)methyl]-4-(2-oxo-2*H*-chromen-3-yl)-7-hydroxy-2*H*-chromen-2-one derivatives [a].

| Cmpd | $NR_2$ | $R^1$ | $R^2$ | *hu*MAO-A | *hu*MAO-B | *ee*AChE | *hu*AChE | *eq*BChE |
|---|---|---|---|---|---|---|---|---|
| **2a** | $NMe_2$ | H | H | **8.30 ± 0.36** | [36 ± 5] | [22 ± 3] | | i.a. |
| **2b** | | Cl | H | **1.49 ± 0.49** | ~10 | ~10 | i.a. | i.a. |
| **2c** | | Br | H | **2.23 ± 0.22** | ~10 | [20 ± 1] | i.a. | i.a. |
| **2d** | | H | OMe | **11.7 ± 1.3** | [28 ± 3] | [39 ± 9] | | [25 ± 3] |
| **3c** | $NEt_2$ | Br | H | **3.04 ± 1.37** | [42 ± 3] | **1.56 ± 0.31** | **4.27 ± 0.58** | [37 ± 4] |
| **4a** | $N(nPr)_2$ | H | H | [29 ± 6] | [33 ± 1] | [37 ± 3] | | [22 ± 3] |
| **4d** | | H | OMe | [29 ± 5] | [43 ± 5] | **3.05 ± 0.97** | **0.97 ± 0.20** | [14 ± 10] |
| **5a** | N(Me)nBu | H | H | [32 ± 3] | [23 ± 3] | [28 ± 3] | | [27 ± 2] |
| **5b** | | Cl | H | **1.85 ± 0.11** | ~10 | [25 ± 5] | ~10 | [17 ± 7] |
| **5c** | | Br | H | **2.52 ± 0.70** | ~10 | **4.25 ± 0.5** | | [25 ± 11] |
| **5d** | | H | OMe | [39 ± 4] | ~10 | **7.80 ± 1.92** | | [40 ± 4] |
| **6a** | $N(CH_2CH_2OMe)_2$ | H | H | [32 ± 5] | [29 ± 6] | [37 ± 9] | | [15 ± 4] |
| **6b** | | Cl | H | [45 ± 3] | [35 ± 9] | [16 ± 4] | | i.a. |
| **6d** | | H | OMe | [26 ± 4] | [31 ± 1] | [20 ± 2] | | i.a. |
| **7a** | $N(iBu)_2$ | H | H | [27 ± 2] | [28 ± 4] | ~10 | | ~10 |
| **7d** | | H | OMe | [27 ± 3] | [31 ± 2] | ~10 | | [34 ± 3] |
| **8a** | N(Me)Bn | H | H | [28 ± 4] | ~10 | [40 ± 9] | | [31 ± 4] |
| **8b** | | Cl | H | ~10 | [38 ± 3] | [16 ± 6] | | i.a. |
| **8d** | | H | OMe | [31 ± 4] | [42 ± 3] | ~10 | | ~10 |
| | Clorgiline | | | 0.0025 ± 0.0002 | 2.51 ± 0.45 | | | |
| | Donepezil | | | | | 0.051 ± 0.003 | | 2.71 ± 0.31 |

[a] Enzymes are human *hu*MAOs A and B, electric eel *ee*AChE, and equine (horse serum) *eq*BChE. $IC_{50}$ values (μM, bold) are listed for compounds achieving more than 60% inhibition at 10 μM concentration or % inhibition at 10 μM concentration in square brackets, expressed as mean ± SD of three independent determinations; $IC_{50}$ reported as ~10 for compounds achieving at 10 μM concentration average % inhibition within the range 50–60%; i.a., compounds displaying average % inhibition less than 10% at 10 μM concentration.

A time course of the inhibition kinetics, measured spectrophotometrically as the increase in absorbance at 316 nm of 4-hydroxyquinoline, i.e., the product of MAO-mediated oxidation of kynuramine as a substrate, confirmed the reversibility of enzyme inhibitor binding (Figure S11, Supplementary Materials).

Three further compounds, namely the 6′-Br congeners **2c**, **3c**, and **5c**, proved to act as MAO-A inhibitors with single-digit micromolar $IC_{50}$s. The inhibition potency appeared to depend on the hydrophobicity and steric hindrance of the aminomethyl group at C8. Within the limits of the explored property space, the data suggest that the anti-MAO (preferentially anti-MAO-A) activity is primarily affected by the size of the tertiary amine of the Mannich base at C8. As a trend, tertiary amines with a double-branched alkyl group (subset **7**) or larger than Et (subsets **4**, **6**, and **8**) are less tolerated than $NMe_2$ (**2**), $NEt_2$ (**3**), and N(Me)*n*Bu (**5**). The halogens at C6′ appear to enhance MAO-A inhibition potency, with Cl exerting a slightly stronger effect than Br. In contrast, the introduction of a methoxy group at C8′ decreases the inhibitory activity against MAO-A.

Regarding the cholinesterase inhibition, most of the screened derivatives proved to preferentially inhibit *ee*AChE over *eq*BChE. Only four compounds (**3c**, **4d**, **5c**, and **5d**) achieved finite $IC_{50}$ values at concentrations less than 10 μM. The most potent *ee*AChE inhibitor was **3c** ($IC_{50}$ 1.56 μM), which also exhibited MAO-A inhibition at a very close $IC_{50}$ (3.04 μM). The optimal AChE inhibition potency was achieved for -$CH_2NEt_2$ and -$CH_2N$*n*$Pr_2$ at C8, with 6′-Br (**3c** and **5c**) or 8′-OMe (**4d** and **5d**) exerting favorable effects.

Compounds **2b**, **2c**, **3c**, **4d**, and **5b**, tested as *hu*AChE inhibitors, confirmed the activity trend observed with *ee*AChE. Interestingly, the 8′-OMe congener **4d** achieved an $IC_{50}$ value of 0.97 μM.

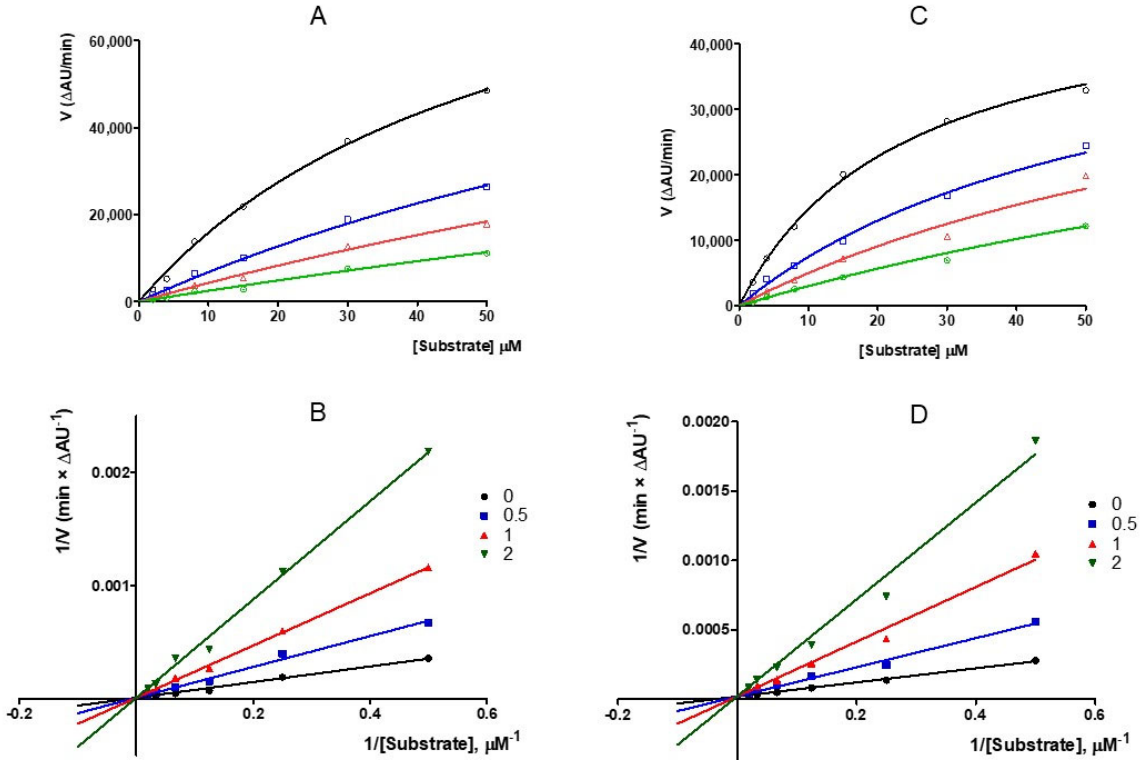



**Figure 2.** Michaelis–Menten (**A**,**C**) and Lineweaver–Burk (**B**,**D**) plots of inhibition kinetics of MAO-A for compounds **2b** (**A**,**B**) and **5b** (**C**,**D**).

Overall, in the series examined, **3c** appears to be the one that inhibits both MAO-A and AChE with a single-digit micromolar $IC_{50}$ and a slight selectivity over MAO-B and BChE, respectively.

### 2.2.2. Molecular Docking Calculations

To shed light on the molecular factors mainly responsible for the more efficient binding modes and higher inhibition potencies of the examined amphoteric biscoumarins to the target enzymes, molecular docking calculations were carried out using AutoDock software (release 4.2). The main results obtained from the docking simulation of most of the compounds with a crystal structure of human MAO-A, in complex with clorgiline (pdb 2BXR), or human MAO-B (pdb 1GOS) are reported in the Supplementary Materials (Table S1), whereas in Table 2, the main docking calculation results are summarized, which pertain to the highest-scored docking poses to MAO-A of **2a**, **2b**, **2d**, **4a**, **5a**, and **5b**, which can help in understanding the key factors modulating the inhibition potency of the compounds under investigation.

In Table 2, besides the free energy of binding (FEB, kcal·mol$^{-1}$), the residues involved in H-bonding, and hydrophobic/aromatic and ionic interactions with the ligand are reported. To aid in the interpretation of the potency ranking, the residues that were established as playing a role in substrate and inhibitor selectivity are highlighted in bold [32]. The 2D graphical representations of the best-scored docking pose of the lead **2a** ($NR_2$ = $NMe_2$, Figure 3), compared to those of the less active **4a** ($NR_2$ = N(*n*Pr)$_2$, Figure 4), could suggest why and how the different MAO-A inhibitory potency may relate to the diverse binding mode.

**Table 2.** Molecular docking results with MAO-A (pdb 2BXR).

| Cmpd | Free Energy of Binding (kcal·mol$^{-1}$) [a] | H-Bonding [b] | Hydrophobic/ Aromatic Interactions [b] | Ionic Interactions [b] |
|---|---|---|---|---|
| **2a** | −11.38 | Ile207, Ser209, Tyr447 | **Phe208**, Leu337, Tyr407, **Tyr444** | Glu216 |
| **2b** | −11.25 | Ser209, **Tyr444** | Ala68, **Tyr407**, The352, **Phe208**, Tyr68, Met350, Ile180, Val93, **Ile335** | - |
| **2d** | −7.62 | Met445 | Thr52, **Tyr44** | - |
| **4a** | −10.06 | Tyr69, Ser209, **Tyr407** | **Phe208**, Val303, **Ile335**, Phe352, **Tyr444**, Met445 | **Tyr407** |
| **5a** | −7.82 | Ser209, Ile207 | Leu97, **Phe208**, Leu337 | - |
| **5b** | −10.98 | Ser209, **Tyr444** | Tyr68, Ala68, Ile180, **Phe208**, Met350, **Ile335** | - |
| Moclobemide | −8.92 | Ser209, **Tyr444** | Leu97, **Phe208**, Ile325, **Ile335**, Leu337 | - |

[a] Free energy of binding (kcal·mol$^{-1}$) estimated by AutoDock 4.2 software for ligands in the highest-scored binding pose. [b] Residues in the binding site of MAO-A mainly involved in the interaction with biscoumarin ligands; residues established as playing a role in substrate and inhibitor selectivity are highlighted in bold.

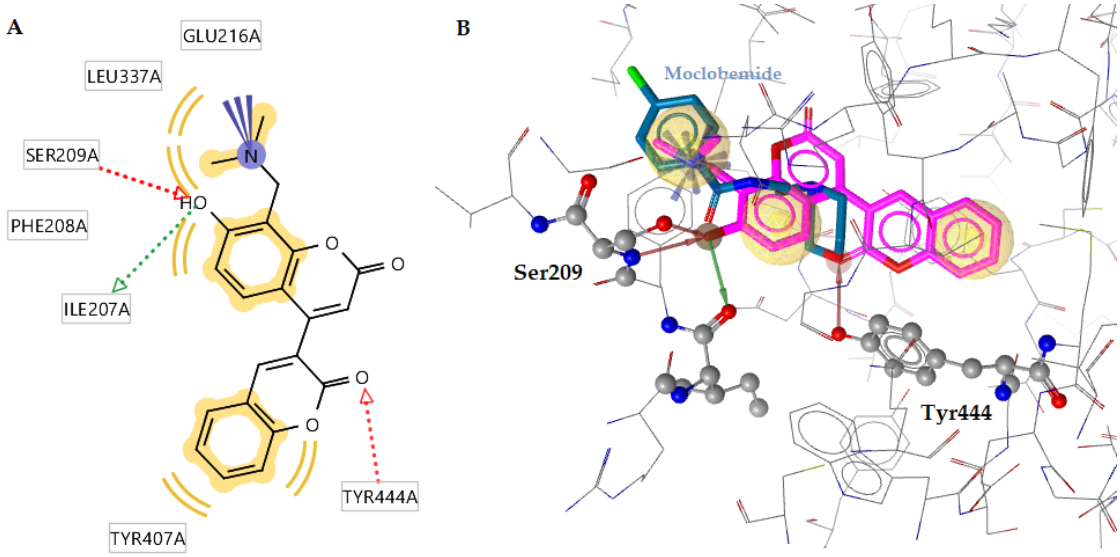



**Figure 3.** (**A**) Two-dimensional diagram of the lead compound **2a** into the MAO-A binding site. (**B**) Superposition of the structure of **2a** (pink) and moclobemide (blue), a well-known selective MAO-A inhibitor, into the active site of the MAO-A enzyme. For clarity, he H atoms have been removed. Red (donor) and green (acceptor) dotted or solid arrows indicate H-bond interactions, and yellow curved lines (**A**) or spheres (**B**) hydrophobic interactions.

Unlike MAO-B, whose FAD binding site has two distinct cavities, i.e., the entrance and substrate cavities separated by a gate (Tyr326), MAO-A has one single hydrophobic cavity (about 550 Å$^3$ volume), in which Phe208 and Ile335 play significant roles in substrate and inhibitor selectivity, whereas Tyr407 and Tyr444 may favor ligand binding through aromatic stacking or H-bond formation through their phenolic OH groups [33].

By orienting the coumarin moiety into a flexible cavity primarily lined by Phe208 and Val210 through hydrophobic contacts, the biscoumarin **2a** may bind MAO-A strongly. The coumarin benzene ring is well accommodated into the catalytic cleft facing the FAD cofactor (Figure 4) by the formation of stable hydrogen bonding through Tyr444 (1.59 Å). Two residues, namely Ser209 and Ile207, should contribute to stabilizing the complex interacting

with the phenolic OH at C7 of the inhibitor as the H-bond donor (2.87 Å) and acceptor (3.05 Å), respectively. Moreover, the protonated tertiary amine of **2a** may attain a salt bridge strengthened by H-bonds with Glu216. In addition, several hydrophobic residues, such as Phe208, Val303, Ile335, Phe352, Tyr444, and Met445, should form extra hydrophobic interactions with the inhibitor into the active site (Figure 3A). The drug moclobemide, taken as a reference MAOAI, exhibited a similar binding mode (Figure 3B). Figure 3 highlights an almost parallel aromatic stacking between flavin and distal coumarin moiety.

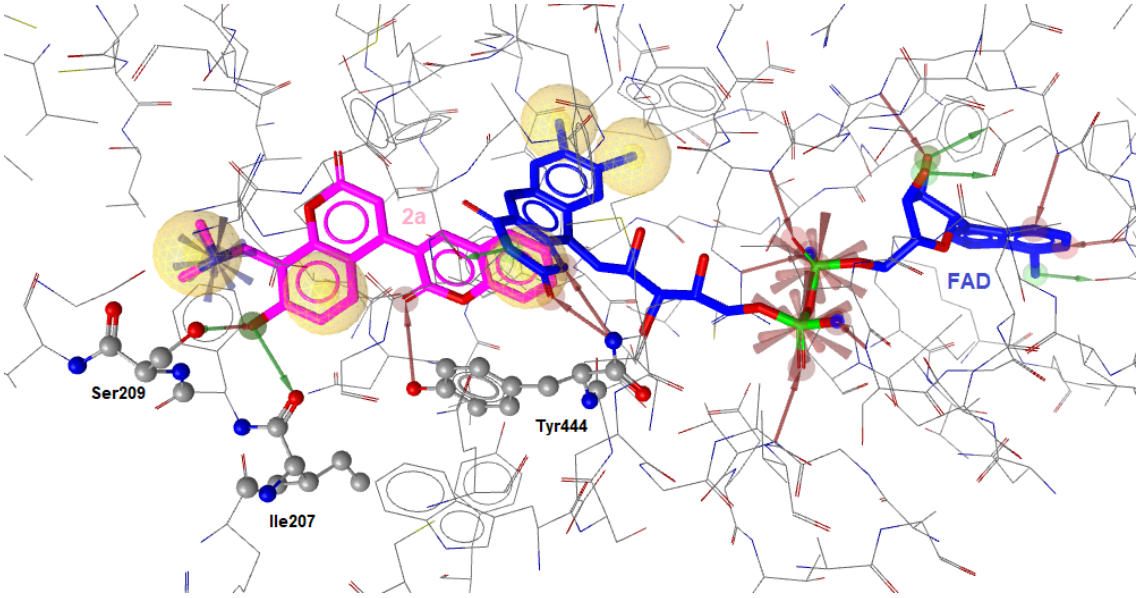



**Figure 4.** The highest-scored docking pose of the biscoumarin compound **2a** (pink) and FAD (blue) into the active site of the MAO-A enzyme. For clarity, the H atoms have been removed. Red (donor) and green (acceptor) solid arrows indicate H-bond interactions, and yellow spheres hydrophobic interactions.

With the increasing size of the alkyls on the tertiary amino groups beyond the ethyl groups, like in **4a** (Figure 5), it can be reasonably hypothesized that the potency decrease could be due to a change in the binding mode with a decrease in the ligand efficiency. Indeed, the interactions of the *n*-propyl groups of the tertiary amine in **4a** with the hydrophobic residues (Tyr444, Met445, Val 303, Phe352) most likely do not compensate the loss of electrostatic interactions and H-bonding achieved by the $NMe_2$ group with Glu216. In addition to the hydrophobic and aromatic interactions around the two coumarin moieties, two key interactions characterize the different (less efficient) binding mode of **4a** compared to that of the more active **2a**, i.e., Ser209 as the H-bond donor to the carbonyl O of the second coumarin nucleus (instead of the phenolic OH) and Tyr407 as the H-bond donor to the O of the first coumarin nucleus.

Compound **2b** (6′-Cl congener) achieved higher activity against MAO-A compared to the unsubstituted **2a** (Figure 6). Similarly to moclobemide, it forms two key H-bonds with active site residues Ser209 and Tyr444, which suggests a similar binding mode. Moreover, the presence of the 6′-Cl substituent appears to enhance binding by stabilizing the molecule within the enzyme's active site, through a halogen bond interaction with Gly66, which might contribute to a more favorable orientation and interaction profile (Figure 6A). In contrast, compound **2d** (8′-OMe congener) shows a different orientation in the active site (Figure 6B) and a less efficient binding mode. The 8′-OMe group is directed toward the core of the binding pocket in an unfavorable conformation, disrupting optimal positioning and weakening key interactions (Figure 6C). This might likely explain its reduced activity compared to **2b**.

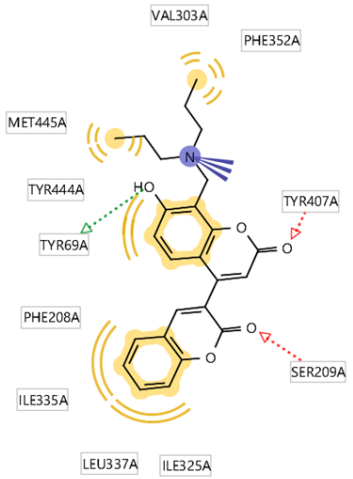



**Figure 5.** Two-dimensional diagram of compound **4a** into the binding site of MAO-A. Red (donor) and green (acceptor) dotted arrows indicate H-bonds, and yellow shadow curved lines hydrophobic interactions.

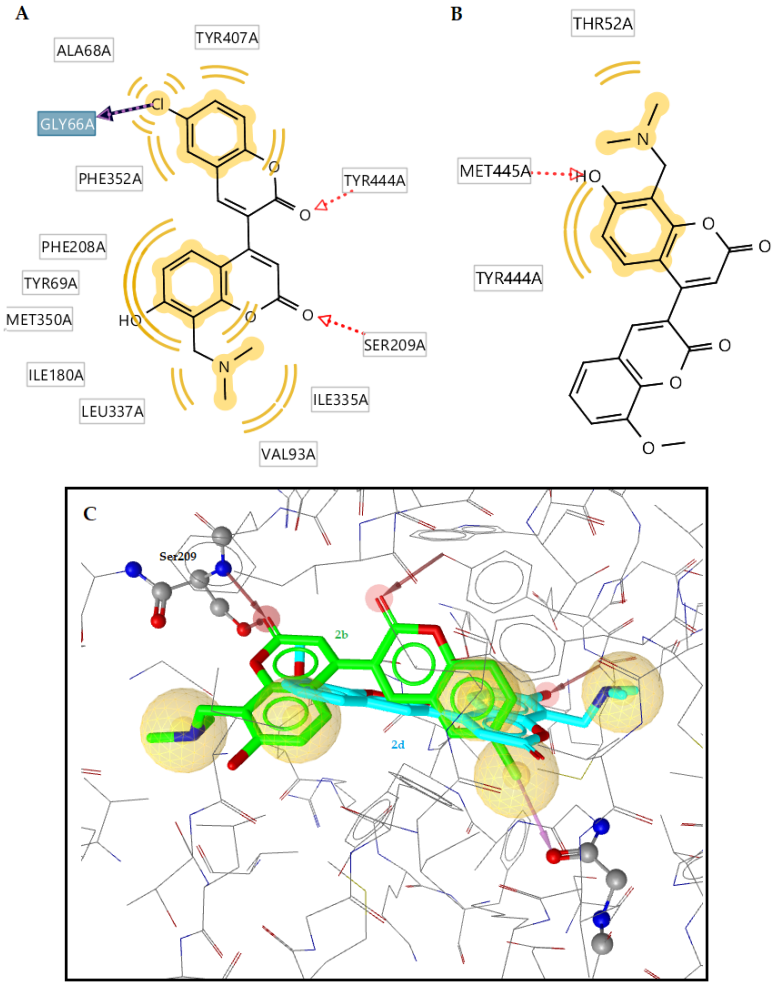



**Figure 6.** (**A**) Two-dimensional diagram of compound **2b** in the binding site of MAO-A. (**B**) Two-dimensional diagram of compound **2d** in MAO-A. (**C**) Superposition of **2b** (green) and **2d** (cyan) in the active site of MAO-A enzyme. Red dotted (**A**,**B**) or solid (**C**) arrows indicate H-bonds, purple halogen bonds, and yellow shadows (**A**,**B**) or spheres (**C**) hydrophobic interactions.

The examined biscoumarin derivatives were also docked against AChE using the crystal structure of the *Torpedo californica* AChE in complex with donepezil (pdb 1EVE). To

validate the docking protocol, donepezil was re-docked using AutoDock, and the resulting RMSD value between the ligand and the re-docked pose was 1.95 Å, which demonstrated the reliability of the docking protocol. Information about all the docking simulations is reported in the Supplementary Materials (Table S2), whereas Table 3 summarizes the results (i.e., free binding energy and the contacting residues) of some selected ligands, including the most potent AChE inhibitor **3c** identified in the series (Figure 7).

**Table 3.** Molecular docking results with AChE (pdb 1EVE).

| Cmpd | Free Binding Energy (kcal·mol$^{-1}$) [a] | H-Bonding | Hydrophobic/Aromatic Interactions [b] | Ionic Interactions [b] |
|---|---|---|---|---|
| **2a** | −5.12 | - | **Phe331**, **Tyr334** | - |
| **2c** | −2.13 | - | - | - |
| **3c** | −9.15 | Tyr70, Phe228 | **Phe330**, **Phe331**, **Tyr334**, Leu282, **Trp279**, Ile287, **Phe290** | - |
| **4d** | −7.15 | Tyr70 | **Trp279**, **Phe290** | - |
| **5c** | −8.02 | - | **Trp84**, **Trp279**, **Phe290** | - |
| **5d** | −8.51 | **Trp84** | **Trp84**, **Tyr279**, Ile287, **Phe290** | - |
| Donepezil | −9.53 | - | **Trp84**, Ile144 | **Phe330**, **Trp84** |

[a] Free energy of binding (kcal·mol$^{-1}$) estimated by AutoDock 4.2 software for ligands in the highest-scored binding pose. [b] Residues in the binding site of AChE mainly involved in the interaction with biscoumarin ligands. Residues lining the anionic site, acyl pocket, oxyanion hole, and peripheral anionic site, which are well-established as playing a role in substrate and inhibitor selectivity, are highlighted in bold.

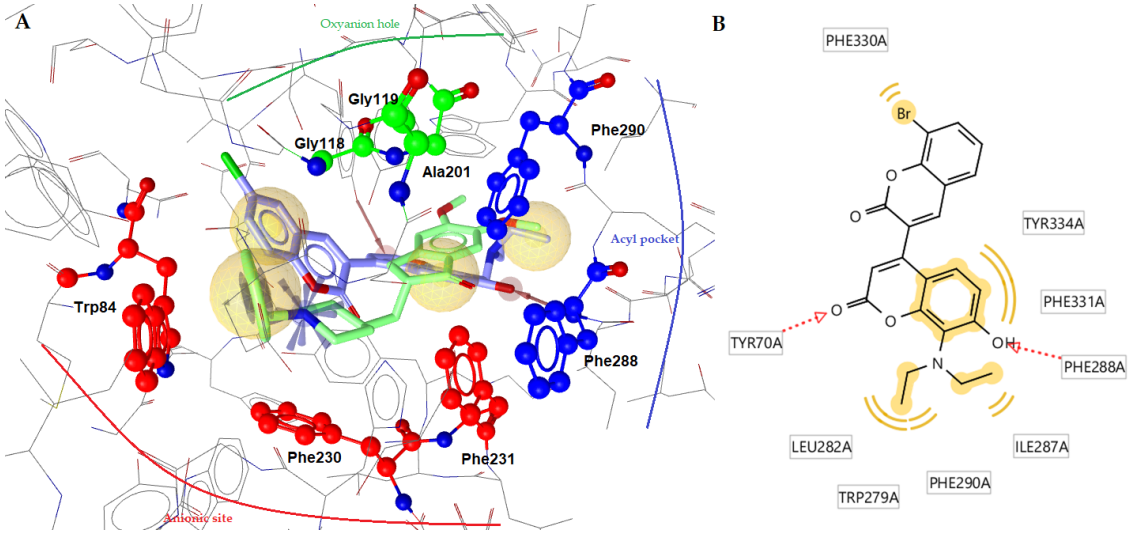



**Figure 7.** (**A**) Superposition of compound **3c** (purple) and donepezil (green) into the active site of AChE. (**B**) Two-dimensional diagram of compound **3c** into the AChE active site. The H atoms have been removed for the sake of clarity. The side chains of the interacting residues are represented as balls and sticks and diversely colored according to the enzyme subsite. Red solid (**A**) or dotted (**B**) arrows indicate H-bonds, and yellow spheres (**A**) or shadow curved lines (**B**) the hydrophobic contacts.

Also in this case, to aid in the interpretation of the docking results, the residues mainly involved in the ligand binding are highlighted in bold, namely Trp84, Phe330, and Phe331 belonging to the anionic site, Phe288 and Phe290 lining the acyl pocket, Gly218, Gly219, and Ala 201 forming the oxyanion hole, and the aromatic residues Trp279, Tyr121, Tyr70, and Tyr334, which together with Asp72 delimit the peripheral anionic site (PAS).

The highest-scored docking pose of donepezil (Figure 7) highlighted the importance of interactions between the dimethoxy phenyl group and Trp279, while the phenyl group

demonstrated aromatic interactions with Trp84. The piperidine N attained arene–cation interactions with Trp84 and Phe330. Hydrophobic interactions were found between donepezil and Ile444 and Tyr84.

Compound **3c**, the most potent AChE inhibitor in the series, showed the best docking score (FEB = −9.15 kcal $mol^{-1}$) and the best binding mode (Figure 7). In the best-scored docking pose, **3c** may form an H-bond between C=O of the first coumarin and Tyr70 (2.54 Å distance) and 7-OH and Phe228 (2.87 Å distance). Moreover, hydrophobic contacts and aromatic stackings with Phe330, Phe331, Tyr334, Leu282, Tyr279, and Ile287 may contribute to the stability of the **3c**-AChE complex.

### *2.3. Physicochemical Properties and Drug-likeness Assessment*

#### 2.3.1. Water Solubility and Lipophilicity Determinations

Aqueous solubility and lipophilicity were experimentally determined for the five compounds for which finite $IC_{50}$ values could be measured within the threshold concentration close to 10 μM (i.e., **2a**–**d** and **3c**). These compounds include the most potent MAO-A inhibitor (**2b**) and the most potent AChE inhibitor (**3c**); the biscoumarin derivative **3c** achieved, on the other hand, the strongest dual enzymes' inhibition with single-digit micromolar $IC_{50}$ values. The kinetic solubility in aqueous buffers was determined in HCl (0.01 M, pH 2.0, KCl 0.15 M) and in PBS (50 mM, pH 7.4, KCl 0.15 M) and at 25 ± 1 °C, using RP-HPLC as the analytical method.

In acidic solution (0.01 M HCl), all the tested compounds achieved a kinetic solubility > $2 \times 10^{-4}$ mol·$L^{-1}$, which means that they can be considered from 'soluble' to 'very soluble' according to the classification of SwissADME based on the topological approach of the ESOL model [34]. In PBS at pH 7.4, the solubilities were found to be two (**2a**) to thirteen (**2c**) to fifty (**3c**) times higher than those calculated with the ESOL model (Table 4), which means that they all fall within the class of 'soluble' compounds (−4 < Log $S$ < −2) and not within the class of 'moderately soluble' compounds (−6 < Log $S$ < −4) as predicted by the ESOL-based calculations for neutral molecules.

**Table 4.** Calculated and experimental solubility and lipophilicity data.

| Cmpd | Solubility (mol/L) | | Lipophilicity | |
|---|---|---|---|---|
| | Calc. [a] | Exp. [b] | Log $P_{calc}$ [c] | Log $k'_w$ [d] |
| **2a** | $8.79 \times 10^{-5}$ | $1.83 \times 10^{-4}$ | 2.96 | 2.11 |
| **2b** | $2.26 \times 10^{-5}$ | $1.47 \times 10^{-4}$ | 3.45 | 2.45 |
| **2c** | $1.08 \times 10^{-5}$ | $1.41 \times 10^{-4}$ | 3.58 | 2.65 |
| **2d** | $7.49 \times 10^{-5}$ | $1.96 \times 10^{-4}$ | 2.94 | 2.32 |
| **3c** | $3.69 \times 10^{-6}$ | $1.81 \times 10^{-4}$ | 4.26 | 2.89 |

[a] Solubility calculated by chemoinformatic tools of the SwissADME free website (http://www.swissadme.ch, accessed on 27 June 2025), applying the topological method (ESOL) implemented by J.S. Delaney [35]. [b] Average solubility (n = 3, RSD < 5%) determined in PBS (50 mM, pH 7.4, 0.15 M KCl) at 25 ± 1 °C. [c] Consensus Log $P_{o/w}$ calculated by SwissADME as the arithmetic mean of octanol/water log Ps calculated by five methods (iLOGP, XLOGP3, WLOGP, MLOGP, and SILICOS-IT), as reported in ref. [34]. [d] Log of the polycratic capacity factor ($k'_w$) determined as lipophilicity parameter by a reversed-phase (RP) HPLC technique [36].

Most likely, such a strong solubility difference between the calculated and experimental values is due to the different degree of ionization at pH 7.4 with respect to minimum solubility at the isoelectric pH, where these amphoteric molecules should exist as zwitterions. Let us compare the ionization-dependent solubility properties of the homologs **2c** and **3c** as examples.

For the amphoteric compound **2c**, ACD/Labs software (release 9.00. version 9.04) estimates $pK_{a1}$ (related to the phenolic OH) and $pK_{a2}$ (related to $CH_2NMe_2$) to be about

9.0 and 7.2, respectively, from which an isoelectric pH of 8.1 is calculated. For the $NEt_2$ homolog **3c**, the estimated p$K_a$ values are about 9.4 and 8.2, and hence an isoelectric pH of 8.8. This could imply that at pH 7.4, the calculated protonated fraction of compound **3c** (0.82), and then its aqueous solubility, is consistently higher than that calculated for **2c** (0.14), despite the decrease in hydrophilicity of their neutral forms. Indeed, in contrast with the expected threefold decrease in water solubility, at pH 7.4, the less hydrophilic **3c** achieves a water solubility 1.3-fold higher than that of **2c**.

The lipophilicity of the five compounds in Table 4 was assessed by calculation and experimental approaches. As a calculated lipophilicity parameter (log $P_{calc}$), we took from the SwissADME free website (http://www.swissadme.ch) the 'Consensus Log $P_{o/w}$', that is, the arithmetic mean of octanol/water log *P*s calculated by five methods (iLOGP, XLOGP3, WLOGP, MLOGP, and SILICOS-IT) [34]. To ascertain the consistency of the calculated log *P* scale, a precise and cost-effective RP-HPLC method [36] was used to determine the polycratic capacity factor (log $k'_w$), that is, the log of the capacity factor ($k'$) extrapolated to 100% water mobile phase, for each compound. The correlation between the RP-HPLC-derived lipophilicity parameter and the predicted log $P_{o/w}$ was proven by the following statistically good linear regression Equation (1):

$$\log k'_w = 0.53\ (\pm 0.10)\ \log P_{calc} + 0.67\ (\pm 0.35)$$
$$n = 5,\ R^2 = 0.900,\ S = 0.110,\ F = 27.08 \quad (1)$$

where $R^2$ is the determination coefficient (i.e., a measure of the explained variance), *S* the standard deviation of the regression model (i.e., a measure of the distance between the observed data points and the regression line), *F* is the F-statistic indicating the overall significance of the regression model, and in parentheses, the 95% confidence intervals of the regression coefficients.

In the above linear equation, the lower-than-unity slope value (+0.53) and the higher-than-zero intercept (+0.67) suggest that retention on the C18 column and partitioning between the immiscible 1-octanol and water are differently influenced by the physicochemical properties of the solutes/analytes. Apparently, the retention of the amphoteric biscoumarins in the RP-HPLC system is affected, not only by the hydrophobic interactions between the long alkyl chains (C18) and the biscoumarin analytes, which in turn dominate in the biphasic partitioning, but also by adsorption and silanophilic interactions, mainly governed by van der Waals interactions, H-bonding, and electrostatic interactions [37]. However, the good statistics associated with the regression equation support the consistency of the relative log $P_{o/w}$ scale assessed by the SwissADME website.

Finally, compounds **2c** and **5c**, taken as representative of the series, were evaluated for their hydrolytic stability in 0.01 M $HCl_{aq}$ (KCl 0.15 M, pH 2.0) and in 0.05 M PBS (KCl 0.15 M, pH 7.4) at 37 ± 1 °C. Sample solutions at 100 μM (DMSO as the cosolvent, 1% *v*/*v*) were incubated at 37 ± 1 °C for 1 h, following shaking of the solution on an orbital shaker at 250 rpm and monitoring by RP-HPLC. Both compounds were found to be stable over 1 h at 37 °C in both conditions.

#### 2.3.2. Chemoinformatic Assessment of Drug-likeness and Bioavailability

For the investigated amphoteric biscoumarins achieving finite $IC_{50}$ values less than (or very close to) 10 μM against MAO-A and/or AChE (**2a**–**d**, **3c**, **4d**, **5b**–**d**), the physicochemical properties, including lipophilicity and water solubility, pharmacokinetics (GI absorption, BBB permeation, and potential as P-gp substrate), drug-likeness (as the compliance with the 'Lipinski's rule of five'), bioavailability, and alerts for pan-assay interference compounds (PAINS) were estimated by querying the free website SwissADME [34] and are summarized in Table S3 (Supplementary Materials).

According to predictions, all nine active compounds achieved a bioavailability score of 0.55, which should suggest a high probability of efficient absorption, with no violation of Lipinski's rule of five and moderate aqueous solubility (at pH 7.4, the experimental water solubility resulted in being even higher, as in the case of the most dual active **3c**). The gastrointestinal absorption is estimated to be high, whereas all the compounds are predicted to be 'not BBB permeant' and, with two exceptions (the 8′-methoxy congeners **4d** and **5d**), to not be P-gp substrates. While solutions for enhancing their BBB crossing can be found at a more advanced stage of lead optimization, exploiting, for instance, novel prodrug approaches or efficient nanoparticle-based drug delivery systems [38], one issue deals with the PAINS alert related to the presence of the Mannich base at C8 of the first coumarin moiety. This alert requires, for sure, attention in the next stages of study. Nevertheless, it has to be highlighted that several safe drugs in various therapeutic areas, including anti-inflammation, anti-infective, and anticancer areas, bear Mannich base groups [39]. An interesting example of a multitarget-directed ligand (MTDL) as a lead candidate for AD is provided by the *ortho*-phenol Mannich base of the anti-inflammatory flurbiprofen [40], which showed good in vitro BBB permeability, low neurotoxicity, biometal-chelating and antioxidant properties, anti-inflammation, and inhibition of Aβ aggregation and AChE. Other phenolic Mannich bases grafted on privileged scaffolds, such as chalcone [41] or 3-benzylidene/benzylphtalide [42], just to name a few, proved to enhance the multifunctional properties of new MTDLs with potential for treating AD.

## 3. Materials and Methods

### *3.1. Chemistry*

#### 3.1.1. General Methods

Starting materials and all chemicals and solvents were purchased from Merck (Darmstadt, Germany). Melting points were determined by using the capillary method on a Stuart Scientific SMP3 electrothermal apparatus (ALT, San Diego, CA, USA) and are uncorrected. Mass spectra were obtained by an Agilent 1100 Series LC–MSD Trap System VL (Agilent Technologies, Santa Clara, CA, USA), equipped with an ESI (electrospray ionization) source, and the high-resolution molecular masses of test compounds were assessed by an Agilent 6530 Accurate Mass Q-TOF spectrometer (Agilent Technologies, Santa Clara, CA, USA). IR spectra (KBr disks) were recorded on a Spectrum One FT infrared spectrophotometer (PerkinElmer, Cambridge, MA, USA), and the most significant absorption bands are listed. $^{1}$H and $^{13}$C NMR spectra were recorded at 400 and 101 MHz, respectively, on a Varian Mercury instrument (Agilent Technologies, Santa Clara, CA, USA) in dimethylsulfoxide-$d_6$ (DMSO-$d_6$) solution at 25 °C. Chemical shifts data are expressed in $\delta$ and the coupling constants $J$ are in hertz (Hz); the following abbreviations are used for multiplicity: s, singlet; br. s, broad singlet; d, doublet; dd, doublet–doublet; td, triplet of doublets; t, triplet; q, quartet; m, multiplet.

Synthesis and characterization of compounds **1a–d** [30,43] have been previously reported.

#### 3.1.2. Synthesis of 8-((Dialkylamino)methyl)-4-(2-oxo-2*H*-chromen-3-yl)-7-hydroxy-2*H*-chromen-2-ones (**2–8**)

To a hot solution of a biscoumarin **1a–d** (2.0 mmol) in dioxane (10 mL), the suitable aminal (2.2 mmol) was added and the mixture was refluxed for 3–5 h. After TLC control, the reaction mixture was cooled and the solvent evaporated under reduced pressure. Finally, the residue crystallized from the *i*-PrOH–*n*-hexane (1:2, *v*/*v*) mixture.

Synthesis and characterization of compounds **4a**, **5a–c**, **6a**, **6b**, **7a**, **7d**, **8a**, and **8b** were published previously [30]. For each newly synthesized compound (**2a–d**, **3c**, **4d**, **5d**, **6d**, and **8d**) uncorrected m.p., main IR bands, $^{1}$H- and $^{13}$C-NMR data, HRMS *m*/*z* are reported

below. $^{1}$H- and $^{13}$C-NMR spectra of the newly synthesized compounds (Figures S1–S9), and the HPLC chromatograms of all the tested compounds (Figure S10) are reported in the Supplementary Material.

*8-((dimethylamino)methyl)-4-(2-oxo-2H-chromen-3-yl)-7-hydroxy-2H-chromen-2-one* (**2a**). m.p.: 208–211 °C; $^{1}$H NMR (400 MHz, DMSO) δ 8.28 (s, 1H), 7.81 (dd, *J* = 7.7, 1.3 Hz, 1H), 7.76–7.68 (m, 1H), 7.51 (d, *J* = 8.2 Hz, 1H), 7.48–7.39 (m, 1H), 7.36 (d, *J* = 8.8 Hz, 1H), 6.67 (d, *J* = 8.8 Hz, 1H), 6.32 (s, 1H), 4.21 (br. s, 1H, OH), 3.96 (s, 2H, $CH_2$), 2.38 (s, 6H, $(CH_3)_2$) ppm; $^{13}$C NMR (101 MHz, DMSO) δ 163.96, 160.39, 159.17, 154.23, 153.15, 151.05, 144.21, 133.21, 129.52, 127.51, 125.28, 123.84, 119.17, 116.74, 113.79, 111.44, 110.03, 108.76, 54.10, 44.37 (2C) ppm; IR (KBr): ν = 3433, 1710, 1737, 1604 cm$^{-1}$; HRMS (Q-TOF): calcd for $C_{21}H_{17}NO_5$ [M − H]$^-$ *m*/*z* 362.1034, found 362.1018, [M + Na]$^+$ *m*/*z* 386.0999, found 386.1002.

*8-((dimethylamino)methyl)-4-(6-chloro-2-oxo-2H-chromen-3-yl)-7-hydroxy-2H-chromen-2-one* (**2b**). m.p.: 210–212 °C; $^{1}$H NMR (400 MHz, DMSO) δ 8.21 (s, 1H), 7.92 (d, *J* = 2.6 Hz, 1H), 7.76 (dd, *J* = 8.9, 2.6 Hz, 1H), 7.56 (d, *J* = 8.9 Hz, 1H), 7.39 (d, *J* = 8.8 Hz, 1H), 6.67 (d, *J* = 8.8 Hz, 1H), 3.97 (s, 2H, $CH_2$, br. s, 1H, OH), 2.38 (s, 6H, $(CH_3)_2$) ppm;$^{13}$C NMR (101 MHz, DMSO) δ 164.09, 160.29, 158.80, 153.19, 152.88, 150.67, 142.89, 132.68, 128.91, 128.44, 127.57, 125.02, 120.59, 118.77, 113.81, 111.43, 109.88, 108.69, 54.06, 44.33 (2C) ppm; IR (KBr): ν = 3420, 1714, 1604, 1574 cm$^{-1}$; HRMS (Q-TOF): calcd for $C_{21}H_{16}ClNO_5$ [M − H]$^-$ *m*/*z* 396.0644, found 396.0642, [M + H]$^+$ *m*/*z* 398.0790, found 398.0788, [M + Na]$^+$ *m*/*z* 420.0609, found 420.0609.

*8-((dimethylamino)methyl)-4-(6-bromo-2-oxo-2H-chromen-3-yl)-7-hydroxy-2H-chromen-2-one* (**2c**). m.p.: 202–204 °C; $^{1}$H NMR (400 MHz, DMSO) δ 8.20 (s, 1H), 8.05 (d, *J* = 2.4 Hz, 1H), 7.87 (dd, *J* = 8.8, 2.4 Hz, 1H), 7.50 (d, *J* = 8.8 Hz, 1H), 7.39 (d, *J* = 8.8 Hz, 1H), 6.66 (d, *J* = 8.8 Hz, 1H), 6.31 (s, 1H), 3.96 (s, 2H, $CH_2$, br. s, 1H, OH), 2.38 (s, 6H, $(CH_3)_2$) ppm; $^{13}$C NMR (101 MHz, DMSO) δ 164.12, 160.29, 158.75, 153.30, 153.18, 150.66, 142.81, 135.45, 131.44, 127.55, 124.96, 121.08, 119.03, 116.61, 113.82, 111.42, 109.87, 108.72, 54.10, 44.34 (2C) ppm; IR (KBr): ν = 3435, 1728, 1714, 1601, 1574 cm$^{-1}$; HRMS (Q-TOF): calcd for $C_{21}H_{16}BrNO_5$ [M − H]$^-$ *m*/*z* 440.0139, found 440.0124, [M + Na]$^+$ *m*/*z* 464.0104, found 464.0194.

*8-((dimethylamino)methyl)-4-(8-methoxy-2-oxo-2H-chromen-3-yl)-7-hydroxy-2H-chromen-2-one* (**2d**). m.p.: 221–225 °C; $^{1}$H NMR (400 MHz, DMSO) δ 8.26 (s, 1H), 7.52–7.24 (m, 4H), 6.67 (d, *J* = 8.8 Hz, 1H), 6.32 (s, 1H), 3.97 (s, 2H, $CH_2$), 3.96 (s, 3H, $OCH_3$), 3.78 (br. s, 1H, OH), 2.39 (s, 6H, N $(CH_3)_2$) ppm; $^{13}$C NMR (101 MHz, DMSO) δ 163.84, 160.35, 158.90, 153.17, 151.02, 146.96, 144.43, 143.59, 127.59, 125.24, 123.99, 120.63, 119.71, 115.45, 113.76, 111.49, 110.05, 108.63, 56.74, 53.96, 44.33 (2C) ppm; IR (KBr): ν = 3430, 1708, 1607, 1384 cm$^{-1}$; HRMS (Q-TOF): calcd for $C_{22}H_{19}NO_6$ [*M* − H]$^-$ *m*/*z* 392.1140, found 392.1133, [M + Na]$^+$ *m*/*z* 416.1105, found 416.1111.

*8-((diethylamino)methyl)-4-(6-bromo-2-oxo-2H-chromen-3-yl)-7-hydroxy-2H-chromen-2-one* (**3c**). m.p.: 198–200 °C; $^{1}$H NMR (400 MHz, DMSO) δ 8.20 (s, 1H), 8.05 (d, *J* = 2.4 Hz, 1H), 7.87 (dd, *J* = 8.8, 2.4 Hz, 1H), 7.49 (d, *J* = 8.8 Hz, 1H), 7.36 (d, *J* = 8.8 Hz, 1H), 6.60 (d, *J* = 8.8 Hz, 1H), 6.28 (s, 1H), 4.09 (s, 2H, $CH_2$), 3.52 (br. s, 1H, OH), 2.71 (q, *J* = 7.2 Hz, 4H, N-$(CH_2CH_3)_2$), 1.11 (t, *J* = 7.2 Hz, 6H, N-$(CH_2CH_3)_2$) ppm; $^{13}$C NMR (101 MHz, DMSO) δ 160.34, 158.75, 153.29, 153.08, 150.69, 142.76, 135.43, 131.43 (2C), 127.32, 125.01, 121.08, 119.03 (2C), 116.69, 114.10, 109.62, 108.50, 49.43, 46.69 (2C), 11.27 (2C) ppm; IR (KBr): ν = 3433, 1731, 1602, 1378 cm$^{-1}$; HRMS (Q-TOF): calcd for $C_{23}H_{20}BrNO_5$ [M − H]$^-$ *m*/*z* 468.0452, found 468.0432, [M + Na]$^+$ *m*/*z* 492.0417, found 416.0420.

*8-((dipropylamino)methyl)-4-(8-methoxy-2-oxo-2H-chromen-3-yl)-7-hydroxy-2H-chromen-2-one* (**4d**). m.p.: 128–130 °C; $^{1}$H NMR (400 MHz, DMSO) δ 8.25 (s, 1H), 7.47–7.27 (m, 4H), 6.62 (d, *J* = 8.8 Hz, 1H), 6.31 (s, 1H), 4.07 (s, 2H, $CH_2$), 3.96 (s, 3H, $OCH_3$), 3.57 (br., s, 1H, OH), 2.57 (dd, *J* = 8.5, 6.6 Hz, 4H, N-$(CH_2CH_2CH_3)_2$), 1.65–1.46 (m, 4H, N-$(CH_2CH_2CH_3)_2$), 0.87 (t, *J* = 7.4 Hz, 6H, N-$(CH_2CH_2CH_3)_2$) ppm; $^{13}$C NMR (101 MHz, DMSO) δ 164.24, 160.37, 158.90, 153.02, 151.02, 146.96, 144.42, 143.58, 127.30, 125.24, 124.02, 120.63, 119.71, 115.44,

113.86, 111.38, 109.99, 108.89, 56.74, 55.51 (2C), 50.50, 19.34 (2C), 12.05 (2C) ppm; IR (KBr): ν = 3430, 2962, 1712, 1605, 1478,1379 $cm^{-1}$; HRMS (Q-TOF): calcd for $C_{26}H_{27}NO_6$ $[M - H]^-$ $m/z$ 448.1766, found 448.1744, $[M + Na]^+$ $m/z$ 472.1731, found 472.1741.

*8-((butyl(methyl)amino)methyl)-4-(8-methoxy-2-oxo-2H-chromen-3-yl)-7-hydroxy-2H-chromen*-2-one (**5d**). m.p.: 163–165 °C; $^1$H NMR (400 MHz, DMSO) δ 8.25 (s, 1H), 7.46–7.27 (m, 4H), 6.63 (d, *J* = 8.8 Hz, 1H), 6.31 (s, 1H), 4.01 (s, 2H, $CH_2$), 3.96 (s, 3H, $OCH_3$), 3.54 (br. s, 1H, OH), 2.64–2.54 (m, 2H, N-($CH_2CH_2CH_2CH_3$)), 2.32 (s, 3H, N-$CH_3$), 1.54 (dt, *J* = 14.9, 7.4 Hz, 2H, N-($CH_2CH_2CH_2CH_3$)), 1.32 (dq, *J* = 14.5, 7.3 Hz, 2H, N-($CH_2CH_2CH_2CH_3$)), 0.90 (t, *J* = 7.3 Hz, 3H, N-($CH_2CH_2CH_2CH_3$)) ppm; $^{13}$C NMR (101 MHz, DMSO) δ 160.38, 158.90, 151.02, 146.96, 144.40 (2C), 143.59, 127.40, 125.23 (2C), 124.03, 120.63 (2C), 119.71, 115.44, 113.86, 108.68 (2C), 56.74, 56.37, 53.07, 41.24, 28.66, 20.26, 14.22 ppm; IR (KBr): ν = 3437, 2935, 1720, 1603 $cm^{-1}$; HRMS (Q-TOF): calcd for $C_{25}H_{25}NO_6$ $[M - H]^-$ $m/z$ 434.1609, found 434.1618, $[M + Na]^+$ $m/z$ 454.1574, found 454.1586.

*8-((bis(2-methoxyethyl)amino)methyl)-4-(8-methoxy-2-oxo-2H-chromen-3-yl)-7-hydroxy-2H-chromen*-2-one (**6d**). m.p.: 165–167 °C; $^1$H NMR (400 MHz, DMSO) δ 8.26 (s, 1H), 7.54–7.13 (m, 4H), 6.68 (d, *J* = 8.8 Hz, 1H), 6.35 (s, 1H), 4.12 (s, 2H, $CH_2$), 3.96 (s, 3H, $OCH_3$), 3.51 (t, *J* = 5.5 Hz, 4H, ($N\underline{CH_2}$-$CH_2OCH_3$)$_2$), 3.24 (s, 6H, ($NCH_2$-$CH_2O\underline{CH_3}$)$_2$), 2.81 (t, *J* = 5.5 Hz, 4H, ($NCH_2$-$\underline{CH_2}OCH_3$)$_2$) ppm; $^{13}$C NMR (101 MHz, DMSO) δ 162.97, 160.33, 158.89, 153.05, 151.00, 146.97, 144.46, 143.60, 127.34, 125.24, 123.97, 120.64, 119.71, 115.46, 113.63, 111.95, 110.50, 109.75, 69.63 (2C), 58.50 (2C), 56.74, 53.18 (2C), 49.82 ppm; IR (KBr): ν = 3437, 1725, 1600, 1384 $cm^{-1}$; HRMS (Q-TOF): calcd for $C_{26}H_{27}NO_8$ $[M - H]^-$ $m/z$ 480.1664, found 480.1649, $[M + Na]^+$ $m/z$ 504.1629, found 504.1638.

*8-(((benzyl(methyl)amino)methyl)-4-(8-methoxy-2-oxo-2H-chromen-3-yl)-7-hydroxy-2H-chromen*-2-one (**8d**). m.p.: 204–206 °C; $^1$H NMR (400 MHz, DMSO) δ 8.26 (s, 1H), 7.49–7.22 (m, 9H), 6.71 (d, *J* = 8.8 Hz, 1H), 6.36 (s, 1H), 4.02 (s, 2H), 3.96 (s, 3H, $OCH_3$), 3.74 (s, 2H, Bn), 2.23 (s, 3H, $NCH_3$) ppm; $^{13}$C NMR (101 MHz, DMSO) δ 162.73, 160.31, 158.88, 153.20, 150.97, 146.97, 144.48, 143.60, 137.50, 129.73 (2C), 128.94 (2C), 127.99, 127.54, 125.24, 123.95, 120.64, 119.71, 115.46, 113.48, 112.04, 110.59, 109.38, 60.97, 56.74, 51.84 ppm; IR (KBr): ν = 3439, 1723, 1602 $cm^{-1}$; HRMS (Q-TOF): calcd for $C_{28}H_{23}NO_6$ $[M - H]^-$ $m/z$ 468.1453, found 468.1451, $[M + Na]^+$ $m/z$ 492.1418, found 504.1413.

### *3.2. Determination of Kinetic Aqueous Solubility and Lipophilicity*

Water solubility and lipophilicity parameters were measured following previously reported methods [36]. For measuring kinetic solubility in aqueous buffers, a 200 μM sample solution in PBS (50 mM, pH 7.4, KCl 0.15 M), or in HCl (0.01 M, pH 2.00, KCl 0.15 M) prepared from a 10 mM stock solution in DMSO, was incubated at room temperature (25 ± 1 °C) for 2 h while being continuously shaken at 250 rpm on an orbital shaker. The mixture was then separated by centrifugation at 2500 rpm for 3 min. Immediately after filtration, 100 μL of the filtrate was mixed with an equal volume of a 1:1 (*v*/*v*) DMSO and PBS (50 mM, pH 7.4, KCl 0.15 M) or HCl (0.01 M, pH 2, KCl 0.15 M) solution to prevent precipitation from the saturated solution and subsequently analyzed by HPLC. The peak area was compared to a calibration curve of the tested compound in MeOH. The analytical parameters were set as follows. Mobile phase: MeOH/water pH 2.8 (acetic acid 0.5% *v*/*v*) at different percentages depending on the retention time of each test compound; stationary phase: Phenomenex, Kinetex 5 μ, C8, (150 × 3 mm); flux: 0.5 μL/min; injection: 2 μL; λ 330 nm. The analyses were performed on the Agilent HPLC 1260 Infinity Series Integrated System (Agilent Technologies, Milan, Italy).

The lipophilicity parameters were determined by an RP-HPLC technique [36]. In short, methanolic solutions of the examined compounds (1 mg·$mL^{-1}$) were analyzed by the Agilent 1260 infinite HPLC system (Agilent Technologies, Milan, Italy) equipped

with a diode array detector (DAD), using a Phenomenex C18-column (Kinetex 5 μ, 100 Å, 150 × 3 mm) as the stationary phase and MeOH/water buffer mobile phases with different $v/v$ composition (i.e., mobile phases containing 0.05 increments of MeOH volume fractions in 10 mM ammonium formate buffer at pH 4.5; $\varphi_{MeOH}$ ranging between 0.70 and 0.20). The chromatographic measurements were carried out at 25 ± 1 °C, flow rate of 0.5 mL·min$^{-1,}$ and detection at λ 330 nm. The log of capacity factors of each compound at different mobile phase compositions was calculated ($\log k' = \log (t_R - t_0)/t_0$, where $t_R$ represents the retention time of the solute and $t_0$ is the column dead time). For each compound, the equation of the linear relationship between $\log k'$ and $\varphi_{MeOH}$ ($R^2 > 0.991$) on at least five datapoints, each from duplicate, was derived by regression analysis and the intercept at the $y$-axis (i.e., $\varphi_{MeOH} = 0$) calculated as the lipophilicity parameter $\log k'_w$.

### *3.3. Enzyme Inhibition Assays*

#### 3.3.1. Inhibition of Monoamine Oxidases

The inhibition assays of human monoamine oxidases were conducted using a fluorescence-based method with kynuramine as a non-selective substrate for each isoform, MAO-A/B [44–46]. Recombinant human MAO-A and MAO-B (microsomes from insect cells infected with baculovirus; Sigma Aldrich, St. Louis, MO, USA) (Merk Life Science S.r.l., Milan, Italy) were used. The measurements were performed in triplicate in black round-bottom polystyrene 96-well plates (Greiner Bio-One, Kremsmünster, Austria). Fluorescence readings were performed using an Infinite M1000 Pro plate reader (Tecan, Cernusco sul Naviglio, Milano, Italy), and inhibition values were calculated using Prism (version 5.01 for Windows; GraphPad Software, San Diego, CA, USA). To evaluate enzymatic activity, clorgiline (a selective MAO-A inhibitor) and selegiline (a selective MAO-B inhibitor) were employed as positive controls. In the MAO inhibition assays, all compounds were initially screened at a concentration of 10 μM. Each of them was preincubated at 37 °C for 20 min with 50 μM kynuramine in a phosphate buffer (PBS, 0.1 M, pH 8.0), adjusted to 0.39 osmolarity with KCl. After adding recombinant human MAO-A/B (250 U/mg and 59 U/mg, respectively) and incubating for another 30 min, NaOH was added. The fluorescence was measured at excitation/emission wavelengths of 310/400 nm. Compounds showing at least 60% MAO inhibition at 10 μM were further tested at seven different concentrations to determine the $IC_{50}$ value, calculated via nonlinear regression. The $IC_{50}$ is reported as the mean ± SD of three independent experiments, each performed in duplicate.

#### 3.3.2. Inhibition of Cholinesterases

Cholinesterase inhibition assays were carried out using the Ellman spectrophotometric method, modified for a 96-well plate format [45,47]. Acetylcholinesterase from electric eel and butyrylcholinesterase from equine serum (Sigma Aldrich) were employed. The measurements were performed in triplicate using clear, flat-bottom polystyrene plates (Greiner Bio-One). To assess enzymatic activity, donepezil (AChE-selective) and tacrine (BChE-selective) were used as positive controls. The solutions containing AChE (1.2 U/mL) or BChE (2 U/mL), 5,5′-dithiobis(2-nitrobenzoic acid) (Ellman's reagent, 0.33 mM), the test compound (10 μM concentration for the initial screening, or seven different concentrations for compounds achieving > 60% enzyme inhibition at 10 μM to determine the $IC_{50}$ value), in PBS (0.1 M, pH 8.0), were incubated for 20 min at 25 °C. Then, acetylthiocholine or butyrylthiocholine iodide (5 μM) as a substrate was added, and the hydrolysis rates were recorded for 5 min at 412 nm. The $IC_{50}$ value, calculated using the nonlinear regression method 'log[inhibitor] vs. response', or % inhibition at 10 μM, is reported as the mean ± SD of three independent experiments, each performed in duplicate.

### 3.4. Molecular Docking Calculations

To comprehend the molecular binding mechanisms of the active compounds toward two distinct biological targets that are associated with human monoamine oxidase enzymes, molecular docking studies were conducted. The human MAO-A (PDB code 2BXR) and human MAO-B (PDB code 1GOS) crystallographic structures from the Protein Data Bank [48] (PDB) were taken into consideration as the enzyme targets for the docking simulations. In the docking simulations, the proteins were considered without co-crystallized ligands. The docking protocol was validated by performing the simulation with only the bound ligands and low RMSD between the docked and crystal conformations, prior to screening the active compounds.

Specifically, the FAD cofactor was retained in the binding sites of both MAO-A and MAO-B to preserve the integrity of the catalytic pocket. In addition, the docking protocol was validated by re-docking the co-crystallized ligands (clorgyline for MAO-A and safinamide for MAO-B), obtaining RMSD values < 2.0 Å between the docked and crystallographic geometries, which confirmed the reliability of the docking setup. The quality of the structural models of the target enzymes was assessed using Ramachandran plots generated by MolProbity (http://molprobity.biochem.duke.edu/help/about.html, accessed on 13 February 2025). For MAO-A (PDB 2BXR), 89.2% of residues (783/878) were in favored regions, while 98.1% (861/878) fell within allowed regions. A total of 17 residues were identified as outliers, mainly clustered in loop segments (e.g., residues 61, 107–109, 118, 215, and 252 in both chains) and including a single glycine (428) and glutamate (399). Outliers in proline and glycine are not uncommon due to their conformational flexibility, and in this structure, they are positioned away from the active site, with no effect on the overall fold or the geometry of the catalytic pocket. The binding environment around the FAD cofactor and the substrate cavity remains well defined, supporting its suitability for molecular docking. In contrast, acetylcholinesterase (PDB 1EVE) exhibited higher stereochemical quality, with 94.2% of residues (501/532) in favored regions and 100% (532/532) in allowed regions, and no outliers detected. Taken together, these results indicate that while MAO-A shows a modest fraction of outliers compared to AChE, the deviations are restricted to flexible, non-critical regions, and the structural quality is sufficient to provide a reliable receptor model for docking studies.

The ligands' structures were prepared by drawing them in Chemdraw 12.0 software. All docking calculations were performed using AutoDock 4.2 [46] software. The docking input files were created, and the docking outcomes were analyzed using the AutoDock Tools software. A 90 × 90 × 90 grid box was created, covering nearly the whole surface of the protein, with grid points spaced 0.375 Å apart. Before the computations, all non-polar hydrogens and crystallographic water molecules were eliminated. The mass center of the TSA that was bound served as the docking grid's center. Using genetic algorithm searches, 100 docked structures were produced in each case.

A default protocol was used, with an initial population of 50 randomly arranged conformations. Heavy atom comparison root mean square deviations (RMSD values) were determined and initial ligand binding modes were plotted. Plots of protein–ligand interactions were generated using LigandScout software (vers. 2.0) [49].

### 3.5. Drug-likeness and Bioavailability Assessment

Physicochemical properties, such as the topological polar surface area (TPSA), consensus logarithm of partition coefficient (Log $P_{o/w}$), and water solubility (Log $S$), pharmacokinetics, ADME-related features, and drug-likeness of the investigated compounds were estimated using the free web server SwissADME [34].

## 4. Conclusions

Evaluating the inhibitory activity of MAOs and ChEs of nineteen amphoteric 3,4′-biscoumarins bearing a (dialkylamino)methyl group at C8 and a phenolic hydroxyl at C7 of the coumarin core, some compounds proved to act as moderate inhibitors of MAO-A and/or AChE with a single-digit micromolar $IC_{50}$. Structure–activity relationships (SARs) suggested that the enzymes' inhibitory potency depends upon the bulkiness and hydrophobicity of the tertiary amino head of the *ortho*-phenolic Mannich base. Indeed, the highest inhibition potency against MAO-A ($IC_{50}$ = 1.49 μM) was achieved by the 8-(dimethylamino)methyl derivative **2b** (6′-Cl congener), whereas the 8-(diethylamino)methyl derivative **3c** (6′-Br congener) exhibited the highest inhibition potency against AChE ($IC_{50}$ = 1.56 μM) as well as a good inhibition of MAO-A ($IC_{50}$ = 3.04 μM).

Even though MAO-B inhibition is recognized as a mechanism contributing to treating PD and AD, selective MAO-A inhibitors could be used to treat depressive forms often associated with the early phases of cognitive decline related to AD [50]. In this study, molecular docking calculations provided support in understanding the key interactions responsible for MAO-A inhibition. The biscoumarin derivative **2b** binds into the MAO-A active pocket in a mode like that adopted by the reference MAO-A selective reversible inhibitor moclobemide forming H-bond interactions with Ser209 and Tyr444, as well as hydrophobic/aromatic interactions; the binding affinity of **2b** is favored by an almost parallel π-stacking between the coumarin-3-yl moiety and the flavin of the cofactor FAD. The most potent AChE inhibitor **3c** in this series achieved the best docking score, but a binding mode quite different from that of the reference drug donepezil. The most potent dual inhibitor **3c**, which can be taken as a hit for future molecular optimization studies and candidate for further AD-related targeted biochemical and biophysical assays (e.g., biometal-chelating, antioxidant, β-amyloid aggregation), showed a good water solubility at pH 7.4 (1.8 mol·$L^{-1}$; fiftyfold more soluble than calculated). Chemoinformatics suggests for **3c** full compliance with Lipinski's rule of five, high probability of gastrointestinal absorption, but low BBB permeation. While further efforts are required to optimize their BBB permeability [51], herein we identified novel phenolic Mannich bases of 4-(2-oxo-2*H*-chromen-3-yl)-2*H*-chromen-2-one as potential MTDLs for treating AD and neurodegenerative syndromes. To this aim, new experiments will be carried out, including Aβ/tau protein aggregation and cell-based neuroprotection assays, on new derivatives identified in the ongoing molecular optimization study, whose results will be reported in due course.

**Supplementary Materials:** The supporting information can be downloaded at: https://www.mdpi.com/article/10.3390/ijms262010197/s1.

**Author Contributions:** Conceptualization, A.G., V.G.K. and C.D.A.; methodology, A.P., C.D., R.P. and B.L.; software, A.P. and M.d.C.; validation, A.P., M.C. and M.d.C.; formal analysis, R.P., C.D. and A.G.; investigation, M.C., V.G.K. and A.N.K.; resources, M.d.C.; data curation, C.D., A.P. and R.P.; writing—original draft preparation, A.G., A.P., C.D. and C.D.A.; writing—review and editing, all the Authors; visualization, all the Authors; supervision, A.G. and C.D.A. All authors have read and agreed to the published version of the manuscript.

**Funding:** This research received no external funding.

**Institutional Review Board Statement:** Not applicable.

**Informed Consent Statement:** Not applicable.

**Data Availability Statement:** The original contributions presented in this study are included in the article and Supplementary Materials. Further inquiries can be directed to the corresponding authors.

**Acknowledgments:** R.P. and M.d.C. acknowledge a support by the Italian Ministry of Universities and Research (PRIN, Grant 202297LJZK_003).

**Conflicts of Interest:** Author Victor G. Kartsev was employed by the company InterBioScreen Ltd. The remaining authors declare that the research was conducted in the absence of any commercial or financial relationships that could be construed as a potential conflict of interest.

## References

1. Chen, Z.-R.; Huang, J.-B.; Yang, S.-L.; Hong, F.-F. Role of Cholinergic Signaling in Alzheimer's Disease. *Molecules* **2022**, *27*, 1816. [CrossRef] [PubMed]
2. Llanes, L.C.; Kuehlewein, I.; França, I.V.D.; Da Silva, L.V.; Da Cruz Junior, J.W. Anticholinesterase Agents For Alzheimer's Disease Treatment: An Updated Overview. *Curr. Med. Chem.* **2023**, *30*, 701–724. [CrossRef]
3. Rafe, M.R.; Saha, P.; Bello, S.T. Targeting NMDA Receptors with an Antagonist Is a Promising Therapeutic Strategy for Treating Neurological Disorders. *Behav. Brain Res.* **2024**, *472*, 115173. [CrossRef]
4. Kim, B.-H.; Kim, S.; Nam, Y.; Park, Y.H.; Shin, S.M.; Moon, M. Second-Generation Anti-Amyloid Monoclonal Antibodies for Alzheimer's Disease: Current Landscape and Future Perspectives. *Transl. Neurodegener.* **2025**, *14*, 6. [CrossRef]
5. Roy, K. (Ed.) *Multi-Target Drug Design Using Chem-Bioinformatic Approaches*; Methods in Pharmacology and Toxicology; Springer: New York, NY, USA, 2019; ISBN 978-1-4939-8732-0.
6. Roy, R.G.; Mandal, P.K.; Maroon, J.C. Oxidative Stress Occurs Prior to Amyloid Aβ Plaque Formation and Tau Phosphorylation in Alzheimer's Disease: Role of Glutathione and Metal Ions. *ACS Chem. Neurosci.* **2023**, *14*, 2944–2954. [CrossRef]
7. Dostert, P.L.; Benedetti, M.S.; Tipton, K.F. Interactions of Monoamine Oxidase with Substrates and Inhibitors. *Med. Res. Rev.* **1989**, *9*, 45–89. [CrossRef]
8. Tripathi, A.C.; Upadhyay, S.; Paliwal, S.; Saraf, S.K. Privileged Scaffolds as MAO Inhibitors: Retrospect and Prospects. *Eur. J. Med. Chem.* **2018**, *145*, 445–497. [CrossRef] [PubMed]
9. Sblano, S.; Boccarelli, A.; Mesiti, F.; Purgatorio, R.; De Candia, M.; Catto, M.; Altomare, C.D. A Second Life for MAO Inhibitors? From CNS Diseases to Anticancer Therapy. *Eur. J. Med. Chem.* **2024**, *267*, 116180. [CrossRef] [PubMed]
10. Pisani, L.; Catto, M.; Muncipinto, G.; Nicolotti, O.; Carrieri, A.; Rullo, M.; Stefanachi, A.; Leonetti, F.; Altomare, C. A Twenty-Year Journey Exploring Coumarin-Based Derivatives as Bioactive Molecules. *Front. Chem.* **2022**, *10*, 1002547. [CrossRef]
11. Todorov, L.; Saso, L.; Kostova, I. Antioxidant Activity of Coumarins and Their Metal Complexes. *Pharmaceuticals* **2023**, *16*, 651. [CrossRef]
12. Malamati-Konstantina, K.; Dimitra, H.-L. Coumarin Derivatives as Therapeutic Candidates: A Review of Their Updated Patents (2017–Present). *Expert Opin. Ther. Pat.* **2024**, *34*, 1231–1254. [CrossRef]
13. Silva, V.L.M.; Silva-Reis, R.; Moreira-Pais, A.; Ferreira, T.; Oliveira, P.A.; Ferreira, R.; Cardoso, S.M.; Sharifi-Rad, J.; Butnariu, M.; Costea, M.A.; et al. Dicoumarol: From Chemistry to Antitumor Benefits. *Chin. Med.* **2022**, *17*, 145. [CrossRef]
14. Ren, Q.-C.; Gao, C.; Xu, Z.; Feng, L.-S.; Liu, M.-L.; Wu, X.; Zhao, F. Bis-Coumarin Derivatives and Their Biological Activities. *Curr. Top. Med. Chem.* **2018**, *18*, 101–113. [CrossRef] [PubMed]
15. Wu, J.-T.; Lv, S.-M.; Lu, C.-H.; Gong, J.; An, J.-B. Effect of 3,3′-Biisofraxidin on Apoptosis of Human Gastric Cancer BGC-823 Cells. *Trop. J. Pharm. Res.* **2015**, *14*, 1803. [CrossRef]
16. Qian, H.; Wang, B.; Ma, J.; Li, C.; Zhang, Q.; Zhao, Y. Impatiens Balsamina: An Updated Review on the Ethnobotanical Uses, Phytochemistry, and Pharmacological Activity. *J. Ethnopharmacol.* **2023**, *303*, 115956. [CrossRef]
17. Zeng, Z.; Tian, R.; Feng, J.; Yang, N.; Yuan, L. A Systematic Review on Traditional Medicine *Toddalia asiatica* (L.) Lam.: Chemistry and Medicinal Potential. *Saudi Pharm. J.* **2021**, *29*, 781–798. [CrossRef]
18. Buechi, G.; Klaubert, D.H.; Shank, R.C.; Weinreb, S.M.; Wogan, G.N. Structure and Synthesis of Kotanin and Desmethylkotanin, Metabolites of Aspergillus Glaucus. *J. Org. Chem.* **1971**, *36*, 1143–1147. [CrossRef]
19. Qu, D.; Li, J.; Yang, X.-H.; Zhang, Z.-D.; Luo, X.-X.; Li, M.-K.; Li, X. New Biscoumarin Derivatives: Synthesis, Crystal Structure, Theoretical Study and Antibacterial Activity against *Staphylococcus aureus*. *Molecules* **2014**, *19*, 19868–19879. [CrossRef] [PubMed]
20. Chougala, B.M.; Samundeeswari, S.; Holiyachi, M.; Naik, N.S.; Shastri, L.A.; Dodamani, S.; Jalalpure, S.; Dixit, S.R.; Joshi, S.D.; Sunagar, V.A. Green, Unexpected Synthesis of Bis-Coumarin Derivatives as Potent Anti-Bacterial and Anti-Inflammatory Agents. *Eur. J. Med. Chem.* **2018**, *143*, 1744–1756. [CrossRef] [PubMed]
21. Luo, W.; Chang, G.; Lin, D.; Xie, H.; Sun, H.; Li, Z.; Mo, S.; Wang, R.; Wang, Y.; Zheng, Z. 3,3′-((3,4,5-trifluoropHenyl)Methylene)Bis(4-Hydroxy-2H-Chromen-2-One) Inhibit Lung Cancer Cell Proliferation and Migration. *PLoS ONE* **2024**, *19*, e0303186. [CrossRef]
22. Abdallah, R.M.; Hammoda, H.M.; El-Gazzar, N.S.; Ibrahim, R.S.; Sallam, S.M. Exploring the Anti-Obesity Bioactive Compounds of *Thymelaea Hirsuta* and *Ziziphus Spina-Christi* through Integration of Lipase Inhibition Screening and Molecular Docking Analysis. *RSC Adv.* **2023**, *13*, 27167–27173. [CrossRef]

23. Ha, N.X.; Huong, T.T.; Khanh, P.N.; Hung, N.P.; Loc, V.T.; Ha, V.T.; Quynh, D.T.; Nghi, D.H.; Hai, P.T.; Scarlett, C.J.; et al. In Vitro and in Silico Study of New Biscoumarin Glycosides from *Paramignya Trimera* against Angiotensin-Converting Enzyme 2 (ACE-2) for Preventing SARS-CoV-2 Infection. *Chem. Pharm. Bull.* **2024**, *72*, 574–583. [CrossRef]
24. Su, C.-X.; Mouscadet, J.-F.; Chiang, C.-C.; Tsai, H.-J.; Hsu, L.-Y. HIV-1 Integrase Inhibition of Biscoumarin Analogues. *Chem. Pharm. Bull.* **2006**, *54*, 682–686. [CrossRef] [PubMed]
25. Asgari, M.S.; Mohammadi-Khanaposhtani, M.; Kiani, M.; Ranjbar, P.R.; Zabihi, E.; Pourbagher, R.; Rahimi, R.; Faramarzi, M.A.; Biglar, M.; Larijani, B.; et al. Biscoumarin-1,2,3-Triazole Hybrids as Novel Anti-Diabetic Agents: Design, Synthesis, in Vitro α-Glucosidase Inhibition, Kinetic, and Docking Studies. *Bioorg. Chem.* **2019**, *92*, 103206. [CrossRef] [PubMed]
26. Bustamante, D.; Bustamante, L.; Segura-Aguilar, J.; Goiny, M.; Herrera-Marschitz, M. Effects of the DT-Diaphorase Inhibitor Dicumarol on Striatal Monoamine Levels in L-DOPA and L-Deprenyl Pre-Treated Rats. *Neurotox. Res.* **2004**, *5*, 569–577. [CrossRef] [PubMed]
27. Hudáčová, M.; Hamuľaková, S.; Konkoľová, E.; Jendželovský, R.; Vargová, J.; Ševc, J.; Fedoročko, P.; Soukup, O.; Janočková, J.; Ihnatova, V.; et al. Synthesis of New Biscoumarin Derivatives, In Vitro Cholinesterase Inhibition, Molecular Modelling and Antiproliferative Effect in A549 Human Lung Carcinoma Cells. *Int. J. Mol. Sci.* **2021**, *22*, 3830. [CrossRef]
28. Huang, G.-Y.; Cui, H.; Lu, X.-Y.; Zhang, L.-D.; Ding, X.-Y.; Wu, J.-J.; Duan, L.-X.; Zhang, S.-J.; Liu, Z.; Zhang, R.-R. (+/−)-Dievodialetins A−G: Seven Pairs of Enantiomeric Coumarin Dimers with Anti-Acetylcholinesterase Activity from the Roots of Evodia Lepta Merr. *Phytochemistry* **2021**, *182*, 112597. [CrossRef]
29. Pisani, L.; Catto, M.; De Palma, A.; Farina, R.; Cellamare, S.; Altomare, C.D. Discovery of Potent Dual Binding Site Acetylcholinesterase Inhibitors via Homo- and Heterodimerization of Coumarin-Based Moieties. *ChemMedChem* **2017**, *12*, 1349–1358. [CrossRef]
30. Frasinyuk, M.S.; Bondarenko, S.P.; Khilya, V.P. Chemistry of 3-Hetarylcoumarins 3*. Synthesis and Aminomethylation of 7′-Hydroxy-3,4′- Bicoumarins. *Chem. Heterocycl. Comp.* **2012**, *48*, 422–426. [CrossRef]
31. Lagunin, A.; Stepanchikova, A.; Filimonov, D.; Poroikov, V. PASS: Prediction of Activity Spectra for Biologically Active Substances. *Bioinformatics* **2000**, *16*, 747–748. [CrossRef]
32. Geha, R.M.; Chen, K.; Wouters, J.; Ooms, F.; Shih, J.C. Analysis of Conserved Active Site Residues in Monoamine Oxidase A and B and Their Three-Dimensional Molecular Modeling. *J. Biol. Chem.* **2002**, *277*, 17209–17216. [CrossRef]
33. Edmondson, D. The FAD Binding Sites of Human Monoamine Oxidases A and B. *Neurotoxicology* **2004**, *25*, 63–72. [CrossRef]
34. Daina, A.; Michielin, O.; Zoete, V. SwissADME: A Free Web Tool to Evaluate Pharmacokinetics, Drug-Likeness and Medicinal Chemistry Friendliness of Small Molecules. *Sci. Rep.* **2017**, *7*, 42717. [CrossRef] [PubMed]
35. Delaney, J.S. ESOL: Estimating Aqueous Solubility Directly from Molecular Structure. *J. Chem. Inf. Comput. Sci.* **2004**, *44*, 1000–1005. [CrossRef] [PubMed]
36. Nevskaya, A.A.; Purgatorio, R.; Borisova, T.N.; Varlamov, A.V.; Anikina, L.V.; Obydennik, A.Y.; Nevskaya, E.Y.; Niso, M.; Colabufo, N.A.; Carrieri, A.; et al. Nature-Inspired 1-Phenylpyrrolo [2,1-a]Isoquinoline Scaffold for Novel Antiproliferative Agents Circumventing P-Glycoprotein-Dependent Multidrug Resistance. *Pharmaceuticals* **2024**, *17*, 539. [CrossRef]
37. Tan, L.C.; Carr, P.W.; Frechet, J.M.J.; Smigol, V. Liquid Chromatographic Study of Solute Hydrogen Bond Basicity. *Anal. Chem.* **1994**, *66*, 450–457. [CrossRef]
38. Alves, P.A.; Camargo, L.C.; Souza, G.M.D.; Mortari, M.R.; Homem-de-Mello, M. Computational Modeling of Pharmaceuticals with an Emphasis on Crossing the Blood–Brain Barrier. *Pharmaceuticals* **2025**, *18*, 217. [CrossRef] [PubMed]
39. Yamali, C.; Gul, M.; Gul, H.I. Current Pharmaceutical Research on the Significant Pharmacophore Mannich Bases in Drug Design. *Curr. Top. Med. Chem.* **2023**, *23*, 2590–2608. [CrossRef]
40. Liu, H.; Qiang, X.; Song, Q.; Li, W.; He, Y.; Ye, C.; Tan, Z.; Deng, Y. Discovery of 4′-OH-Flurbiprofen Mannich Base Derivatives as Potential Alzheimer's Disease Treatment with Multiple Inhibitory Activities. *Bioorg. Med. Chem.* **2019**, *27*, 991–1001. [CrossRef]
41. Zhang, X.; Song, Q.; Cao, Z.; Li, Y.; Tian, C.; Yang, Z.; Zhang, H.; Deng, Y. Design, synthesis and evaluation of chalcone Mannich base derivatives as multifunctional agents for the potential treatment of Alzheimer's disease. *Bioorg. Chem.* **2019**, *87*, 395–408. [CrossRef]
42. Cao, Z.; Song, Q.; Yu, G.; Liu, Z.; Cong, S.; Tan, Z.; Deng, Y. Novel 3-benzylidene/benzylphthalide Mannich base derivatives as potential multifunctional agents for the treatment of Alzheimer's disease. *Bioorg Med. Chem.* **2021**, *35*, 116074. [CrossRef] [PubMed]
43. Dubovik, I.P.; Garazd, M.M.; Khilya, V.P. Modified Coumarins. 14. Synthesis of 7-Hydroxy-[4,3′]Dichromenyl-2,2′-Dione Derivatives. *Chem. Nat. Compd.* **2004**, *40*, 434–443. [CrossRef]
44. Kulikova, L.N.; Purgatorio, R.; Beloglazkin, A.A.; Tafeenko, V.A.; Reza, R.G.; Levickaya, D.D.; Sblano, S.; Boccarelli, A.; De Candia, M.; Catto, M.; et al. Chemical and Biological Evaluation of Novel 1*H*-Chromeno [3,2-*c*]Pyridine Derivatives as MAO Inhibitors Endowed with Potential Anticancer Activity. *Int. J. Mol. Sci.* **2023**, *24*, 7724. [CrossRef]

45. Titov, A.A.; Purgatorio, R.; Obydennik, A.Y.; Listratova, A.V.; Borisova, T.N.; de Candia, M.; Catto, M.; Altomare, C.D.; Varlamov, A.V.; Voskressensky, L.G. Synthesis of Isomeric 3-Benzazecines Decorated with Endocyclic Allene Moiety and Exocyclic Conjugated Double Bond and Evaluation of Their Anticholinesterase Activity. *Molecules* **2022**, *27*, 6276. [CrossRef]
46. Purgatorio, R.; Candia, M.; Catto, M.; Rullo, M.; Pisani, L.; Denora, N.; Carrieri, A.; Nevskaya, A.A.; Voskressensky, L.G.; Altomare, C.D. Evaluation of Water-Soluble Mannich Base Prodrugs of 2,3,4,5-Tetrahydroazepino [4,3-*b*]Indol-1(6 *H*)-one as Multitarget-Directed Agents for Alzheimer's Disease. *ChemMedChem* **2021**, *16*, 589–598. [CrossRef]
47. Berman, H.M.; Battistuz, T.; Bhat, T.N.; Bluhm, W.F.; Bourne, P.E.; Burkhardt, K.; Feng, Z.; Gilliland, G.L.; Iype, L.; Jain, S.; et al. The Protein Data Bank. *Acta Crystallogr. D Biol. Crystallogr.* **2002**, *58*, 899–907. [CrossRef]
48. Morris, G.M.; Goodsell, D.S.; Halliday, R.S.; Huey, R.; Hart, W.E.; Belew, R.K.; Olson, A.J. Automated Docking Using a Lamarckian Genetic Algorithm and an Empirical Binding Free Energy Function. *J. Comput. Chem.* **1998**, *19*, 1639–1662. [CrossRef]
49. Wolber, G.; Langer, T. LigandScout: 3-D Pharmacophores Derived from Protein-Bound Ligands and Their Use as Virtual Screening Filters. *J. Chem. Inf. Model.* **2005**, *45*, 160–169. [CrossRef] [PubMed]
50. Chai, Y.; Shokri-Kojori, E.; Saykin, A.J.; Yu, M. Anxious-depressive symptoms and sleep disturbances across the Alzheimer disease spectrum. *Nat. Ment. Health* **2025**, *3*, 594–612. [CrossRef]
51. Upadhyay, R.K. Drug delivery systems, CNS protection, and the blood brain barrier. *Biomed. Res. Int.* **2014**, *2014*, 869269. [CrossRef] [PubMed]


**Disclaimer/Publisher's Note:** The statements, opinions and data contained in all publications are solely those of the individual author(s) and contributor(s) and not of MDPI and/or the editor(s). MDPI and/or the editor(s) disclaim responsibility for any injury to people or property resulting from any ideas, methods, instructions or products referred to in the content.